

Infrared and Raman spectroscopy of ZnO nanoparticles annealed in hydrogen

W. M. Hlaing Oo and M. D. McCluskey^{a)}

Department of Physics and Astronomy, Washington State University, Pullman, Washington 99164-2814, USA

J. Huso and L. Bergman

Department of Physics, University of Idaho, Moscow, Idaho 83844, USA

(Received 18 April 2007; accepted 9 July 2007; published online 29 August 2007)

The effect of hydrogen on the conductivity of ZnO nanoparticles has implications for nanoscale optoelectronic devices. In this study, infrared reflectance spectra of as-grown and hydrogen-annealed ZnO nanoparticles were measured at near-normal incidence. The as-grown particles were electrically semi-insulating and show reflectance spectra characteristic of insulating ionic crystals. Samples annealed in hydrogen showed a significant increase in electrical conductivity and free-carrier absorption. A difference was observed in the reststrahlen line shape of the conductive sample compared to that of the as-grown sample. The effective medium approximation was applied to model the reflectance and absorption spectra. The agreement between experimental results and the model suggests that the nanoparticles have inhomogeneous carrier concentrations. Exposure to oxygen for several hours led to a significant decrease in carrier concentration, possibly due to the adsorption of negative oxygen molecules on the nanoparticle surfaces. © 2007 American Institute of Physics. [DOI: 10.1063/1.2773635]

I. INTRODUCTION

Control over the electrical and optical properties of nanoparticles is a key requirement for practical applications of these materials for optoelectronic devices. As the particles approach nanometer dimensions, they possess two important properties: (1) the quantum confinement effect and (2) a large ratio of surface area to volume relative to bulk materials. The latter property is relevant to hydrogen storage and catalysis. Due to their small size, doping levels in semiconductor nanoparticles can be characterized by a discrete number of free carriers,¹ and in some cases, the particles contain no free carriers.² Infrared (IR) reflectance spectroscopy is a useful method to determine free carrier concentrations in semiconductors.^{3,4} In this work, we studied the free carrier concentration in ZnO nanoparticles before and after annealing in hydrogen, using IR spectroscopy. Electrical measurements and Raman spectroscopy complemented the IR experiments.

Zinc oxide (ZnO)^{5,6} is a wide band gap semiconductor that is desirable for many applications. Several IR reflectance spectroscopy studies on ZnO have been performed previously. Collins and Kleinman⁷ measured the reflectivity of bulk samples in the spectral range between 1 and 45 μm . For samples with free carrier concentrations below 10^{16} cm^{-3} , the intrinsic reflectance spectrum of an ionic crystal⁸ was observed. The contribution from free carriers becomes significant when the carrier concentration is larger than $\sim 10^{17} \text{ cm}^{-3}$. The anisotropy of optical parameters of bulk wurtzite ZnO crystals has also been reported.^{9,10} Nan *et*

*al.*¹¹ measured the IR reflectance spectra of ZnO nanoparticles, which provided evidence of low free carrier density.

Hydrogen plays an important role in controlling the electrical conductivity of bulk ZnO.¹² At the nanometer scale, Heo *et al.*¹³ demonstrated that postgrowth annealing in hydrogen can dramatically increase the conductivity of single ZnO nanorods. In the present work, evidence for hydrogen donors in ZnO nanoparticles is presented.

II. EXPERIMENT

The synthesis of ZnO nanoparticles used in this work is similar to that used in previous experiments.^{14,15} The nanoparticles were produced by the reaction of zinc acetate dihydrate $[\text{Zn}(\text{CH}_3\text{COO})_2 \cdot 2\text{H}_2\text{O}]$ with sodium hydrogen carbonate (NaHCO_3) at 200 °C for 3 h. X-ray diffraction and transmission electron microscopy results showed that the particles are 15–20 nm diameter with the hexagonal wurtzite structure.¹⁴ The particles were pressed into 7 mm diameter pellets with a thickness of 0.25 mm. Some of the pellets were sealed in a quartz ampoule filled with 2/3 atm hydrogen and annealed at 350 °C for 1 h.

Reflectance spectra were taken with a near normal reflectance geometry, using a BOMEM DA8 Fourier transform infrared spectrometer. The spectra between 200 and 500 cm^{-1} were obtained with a Mylar beam splitter and deuterated triglycine sulfate (DTGS) detector. A KBr beamsplitter and MgCdTe detector were used for wave numbers above 500 cm^{-1} . A gold mirror was used as a reference.

Complementary results were obtained by electrical conductivity measurements. A standard four-probe conductivity measurement in the van der Pauw geometry was used. Electrical contacts were made by conductive silver paint on the periphery of the samples. Resonance Raman spectra of as-

^{a)} Author to whom correspondence should be addressed; electronic mail: mattmcc@wsu.edu

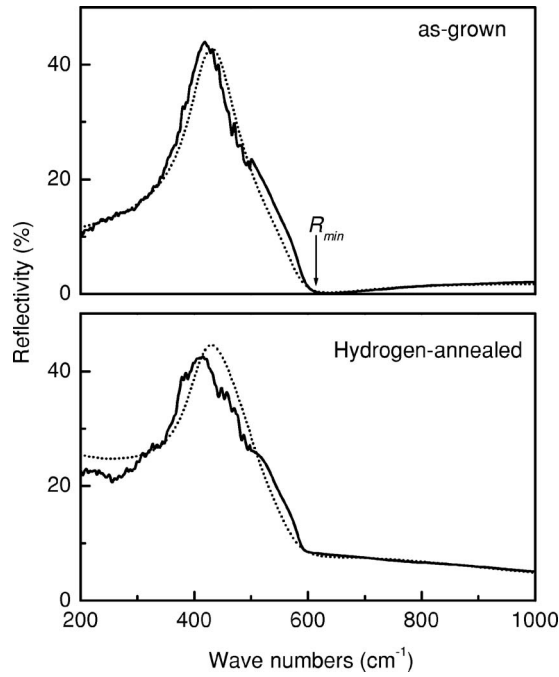


FIG. 1. Infrared reflectance spectra of ZnO nanoparticles. The dotted lines denote the calculated spectra.

grown and hydrogen annealed samples were taken by a continuous wave-Kimmon laser with a wavelength of 325 nm and a JY-Horiba micro-Raman/photoluminescence system. For the IR absorption spectra, hydrogen annealed nanoparticles were dispersed in a KBr matrix (1 and 2% wt.). A pure KBr pellet was used as a reference to minimize the surface scattering effects. To test the effect of ambient gas on the reflectivity of a hydrogen-annealed sample, we used a vacuum tight chamber. The sample was placed in the chamber and the desired gas was supplied (1 atm) after the chamber was evacuated. After a 24 h exposure for each gas, the sample was removed from the chamber and reflectance spectra were recorded.

Secondary ion mass spectrometry (SIMS) was performed on a sample annealed in deuterium at 350 °C for 1 h. The SIMS measurement used a 14.5 keV Cs⁺ ion beam and an implanted silicon sample for deuterium calibration. The sample showed a deuterium concentration of $3 \times 10^{20} \text{ cm}^{-3}$. The deuterium profile was constant down to the maximum depth of the SIMS measurement (8 μm). Although SIMS cannot determine how much hydrogen diffuses into the nanoparticles, our discussion in the next section suggests a doping level in the 10^{19} cm^{-3} range.

III. RESULTS AND DISCUSSION

A. IR reflectance

IR reflectance spectra are shown in Fig. 1 for an as-grown sample and a sample annealed in hydrogen. The reflectivity of the as-grown sample shows a sharp decrease in reflectivity ($R_{\min} \approx 0$) near the longitudinal optical phonon frequency ω_{LO} . This feature is a typical reststrahlen band reflection of semi-insulating ZnO.⁷ The hydrogen annealed sample exhibits a change in the reststrahlen line shape and

the disappearance of R_{\min} was observed. The reflectance change is consistent with an increase in the free carrier concentration. It should be noted that the nanoparticle pellets have a lower overall reflectivity compared to that of bulk ZnO, due to open voids in the sample.¹¹ We repeated measurements with many different samples to ensure consistency and reproducibility. The electrical measurements show that the as-grown pellets are semi-insulating ($\rho \sim 10^7 \text{ } \Omega \text{ cm}$). Hydrogen annealing reduces the resistivity by several orders of magnitude ($\rho \sim 1 \text{ } \Omega \text{ cm}$). This result gives support to the hypothesis that hydrogen annealing leads to an increase in free carrier concentration. Annealing in air or argon gas does not result in any changes in the reflectivity or conductivity of the samples.

B. Modeling

To model the reflectance spectra, the dielectric function of ZnO was calculated by a classical Lorentz–Drude model¹⁶

$$\varepsilon^*(\omega) = \varepsilon_{\infty} \left[1 + \frac{\omega_{\text{LO}}^2 - \omega_{\text{TO}}^2}{\omega_{\text{TO}}^2 - \omega^2 - i\Gamma\omega} - \frac{\omega_p^2}{\omega^2 + i\gamma\omega} \right]. \quad (1)$$

The constants ε_{∞} , ω_{LO} , ω_{TO} , and Γ are the high frequency dielectric constant, longitudinal optical (LO) phonon frequency, transverse optical (TO) phonon frequency, and damping coefficient, respectively. The parameter ω_p is the so-called plasma frequency, which depends on the free carrier concentration n ,

$$\omega_p = \sqrt{\frac{ne^2}{\varepsilon_{\infty}\varepsilon_0 m}}, \quad (2)$$

where e and m are the charge and mass of a free electron, respectively, ε_0 is the permittivity of free space, and γ is an electronic damping coefficient. For a normal incidence geometry, the reflectivity is given by

$$R = \left| \frac{\sqrt{\varepsilon} - 1}{\sqrt{\varepsilon} + 1} \right|^2. \quad (3)$$

The previous expressions are applicable for bulk surfaces, but do not produce satisfactory results for nanoparticle pellets. In nanoparticles, the existence of one free electron in a 20 nm diameter particle yields a free carrier concentration of $n \sim 2 \times 10^{17} \text{ cm}^{-3}$. Since the as-grown sample is semi-insulating, we assumed that some fraction of the particles have no free carriers ($n=0$), and the remaining particles have one electron each ($n \sim 2 \times 10^{17} \text{ cm}^{-3}$). For the hydrogen annealed sample, an additional constituent of heavily doped particles ($n \sim 10^{19} \text{ cm}^{-3}$) was included. This assumption is to simplify the model; in fact, the inhomogeneity of dopants among the nanoparticles is described by a binomial distribution.¹⁷ The dielectric functions for each constituent were calculated using Eq. (1), and the open voids taken as $\varepsilon=1$.

For an inhomogeneous medium, the effective dielectric function ε_{eff} is given by the Bruggeman model¹⁸

TABLE I. Parameters used in calculations (see Sec. III B). Constants are: $\omega_{\text{TO}}=410 \text{ cm}^{-1}$, $\omega_{\text{LO}}=575 \text{ cm}^{-1}$, and $\epsilon_{\infty}=3.7$.

Sample	$f(\%)$	$\omega_p(\text{cm}^{-1})$	$n(\text{cm}^{-3})$	$\gamma(\text{cm}^{-1})$	$\Gamma(\text{cm}^{-1})$
As-grown	30	0	0	...	50
	31	160	2×10^{17}	150	50
Hydrogen-annealed	32	230	6×10^{17}	150	65
	29	1900	4×10^{19}	1350	60
After 1 day	34	230	6×10^{17}	150	60
	27	1800	3.6×10^{19}	1350	60
After 21 days	35	200	4×10^{17}	150	60
	26	1700	3.2×10^{19}	1350	60
Particles in KBr (1% wt.)	0.25	230	6×10^{17}	150	65
	0.275	1900	4×10^{19}	2550	60
Particles in KBr (2% wt.)	0.5	230	6×10^{17}	150	65
	0.44	1900	4×10^{19}	2550	60

$$\sum_j f_j \frac{\epsilon_j - \epsilon_{\text{eff}}}{\epsilon_j + 2\epsilon_{\text{eff}}} = 0, \quad (4)$$

where ϵ_j is the dielectric function of the j th constituent (in our case, ZnO nanoparticles and open voids) with volume fraction f_j , and $\sum_j f_j = 1$. The reflectance spectra were modeled by Eq. (3) with the calculated values ϵ_{eff} . The surface roughness correction was applied by the following equation:¹⁹

$$R = R_0 \exp\left(-\frac{16\pi^2 \delta^2}{\lambda^2}\right), \quad (5)$$

where R and R_0 are reflectivity of the sample with and without surface roughness, respectively. The root-mean-square value of the roughness δ was chosen as an adjustable parameter; $\delta=47 \text{ nm}$ was used in all the fits.

The simulated spectra and parameters used in the fits are presented in Fig. 1 and Table I, respectively. Small discrepancies between the model and experiment are due, in part to, the anisotropy of phonon frequencies and our simplified model of inhomogeneity. Nevertheless, the model is in good agreement with measured reflectance spectra, and it suggests that the nanoparticles have an inhomogeneous free carrier concentration.

Due to their large surface-to-volume ratio, nanoparticles are susceptible to contamination from the ambient. Figure 2 shows reflectance spectra of a hydrogen-annealed sample, measured after the sample was exposed to air. The fits to the IR spectra indicate that the drop in reflectivity is due to a reduction in the fraction of heavily doped particles (Table I).

It is possible that oxygen in ambient air could capture the free carriers in the nanoparticles.²⁰ Nanoparticles have large surface to volume ratios and oxygen molecules can be adsorbed on the surfaces as negatively charged molecules. The adsorbed oxygen molecules transform the n -type nanoparticles to a semiconducting phase. To test this hypothesis, we investigated the stability of the IR reflectivity under different ambients. As shown in Fig. 3, exposure to oxygen gas results the largest drop in the reflectivity. Small changes in

the other spectra may due to adsorption of oxygen from the air as the sample was transferred between the gas chamber and the spectrometer.

Raman spectra of as-grown and hydrogen-annealed ZnO nanoparticles are shown in Fig. 4. Unlike bulk ZnO, LO phonon-plasmon coupling²¹ (LOPC) does not broaden the LO phonon Raman line shape of the doped sample. This may due to the fact that a significant fraction of the nanoparticles are not heavily doped. In addition, it is conceivable that the LOPC strength is lower in nanoparticles than in bulk crystals.

We also measured the IR transmittance of a hydrogen-annealed sample to detect hydrogen local vibrational modes. Unfortunately, the sample was opaque to IR radiation in the spectral range of interest.²² Similar difficulties were also encountered in hydrogen plasma treated ZnO thin films.²³ To address that problem, we mixed small quantities of ZnO in a KBr pellet, as discussed in the next section.

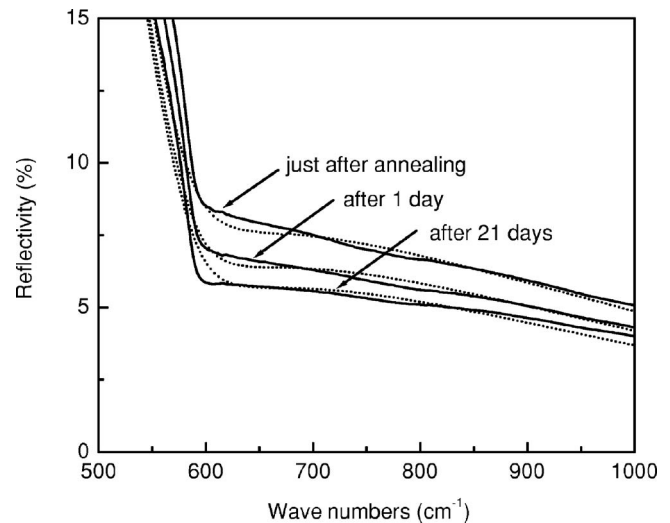


FIG. 2. Reflectivity change after the hydrogen-annealed sample was exposed to air. The dotted lines denote the calculated spectra.

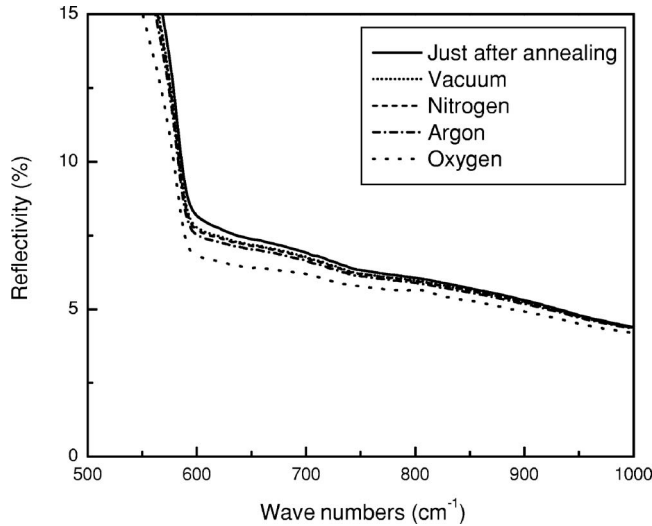


FIG. 3. Reflectivity of the hydrogen-annealed sample after subsequent exposure to vacuum, N₂, Ar, and O₂.

C. IR absorption of hydrogen annealed ZnO nanoparticles

IR absorption spectra (Fig. 5) of hydrogen annealed nanoparticles in a KBr matrix show characteristic free carrier absorption, as absorption increases with wavelength. To model the absorption spectrum, the modified Maxwell-Garnett model²⁴ was chosen, which is appropriate for dilute quantities of ZnO in a KBr host. The effective dielectric function is given by

$$\epsilon_{\text{eff}} = \epsilon_{\text{KBr}} \left(\frac{3 + 2 \sum_j f_j p_j}{3 - \sum_j f_j p_j} \right), \quad (6)$$

where

$$p_j = 3 \left(\frac{\epsilon_j - \epsilon_{\text{KBr}}}{\epsilon_j + 2\epsilon_{\text{KBr}}} \right). \quad (7)$$

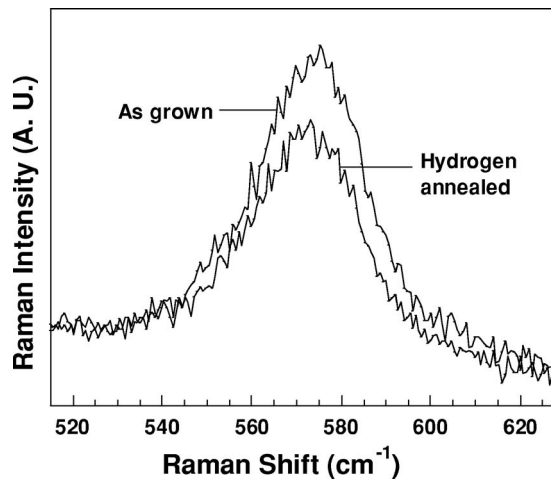


FIG. 4. Raman spectra of ZnO nanoparticles.

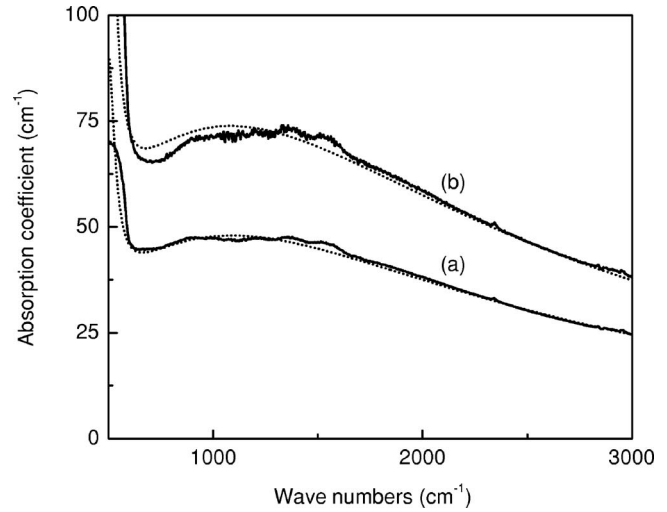


FIG. 5. Infrared absorption spectra of hydrogen-annealed ZnO nanoparticles dispersed in a KBr matrix, with ZnO concentrations of (a) 1% and (b) 2% wt. The dotted lines represent calculated absorption spectra.

The procedure described previously was used to calculate the dielectric function of ZnO nanoparticles (ϵ_j). The dielectric constant for KBr was taken as $\epsilon_{\text{KBr}} = 2.34$. The absorption coefficient α was determined by⁸

$$\alpha = \frac{4\pi\kappa_{\text{eff}}}{\lambda}, \quad (8)$$

where κ_{eff} is the imaginary part of the effective refractive index. The calculated absorption spectra show good agreement with the measured spectra (Fig. 5). The estimated plasma frequencies for the reflectance and absorption spectra are also in good agreement (Table I).

Although hydrogen clearly affects the conductivity of ZnO nanoparticles, we were unable to detect hydrogen related local vibrational modes. The reason for this null result may be that the IR absorption peaks are broad such that the signal is below the noise. Alternatively, hydrogen may modify the nanoparticle and then desorb, resulting in an *n*-type defect such as an oxygen vacancy.

IV. CONCLUSION

In conclusion, we demonstrated the effect of hydrogen annealing on ZnO nanoparticles. IR reflectance and absorption spectra indicate that hydrogen significantly increases the free carrier concentration. The spectra were modeled using the effective medium approximation, given an inhomogeneous free carrier concentration. The large surface area of nanoparticles provides adsorption sites for oxygen molecules that can capture electrons and reduce the free electron concentration. Although the IR spectra show significant differences between as-grown and annealed samples, Raman results do not show a statistically significant difference. These results indicate that IR spectroscopy may provide a superior method for determining the doping level in ZnO nanoparticles.

ACKNOWLEDGMENTS

This work was supported in part by the National Science Foundation under Grant Nos. DMR-0203832 and DMR-0704163, and Department of Energy Hydrogen Initiative Award No. DE-FG02-05ER46251. Acknowledgment is made to Donors of the American Chemical Society Petroleum Research Fund for partial support of this research.

¹P. Verma, G. Irmer, and J. Monecke, *J. Phys.: Condens. Matter* **12**, 1097 (2000).

²N. Y. Morgan, C. A. Leatherdale, M. Drndic, M. V. Jarosz, M. A. Kastner, and M. Bawendi, *Phys. Rev. B* **66**, 075339 (2002).

³T. S. Moss, T. D. Hawkins and G. J. Burrell, *J. Phys. C* **1**, 1435 (1968).

⁴W. Songprakob, R. Zallen, W. K. Liu, and K. L. Bacher, *Phys. Rev. B* **62**, 4501 (2000).

⁵U. Ozgur, Ya. I. Alivov, C. Liu, A. Teke, M. A. Reshchikov, S. Dogan, V. Avrutin, S. J. Cho, and H. Morkoc, *J. Appl. Phys.* **98**, 041301 (2005).

⁶S. J. Pearton, D. P. Norton, K. Ip, Y. W. Heo, and T. Steiner, *Prog. Mater. Sci.* **50**, 293 (2005).

⁷R. J. Collins and D. A. Kleinman, *J. Phys. Chem. Solids* **11**, 190 (1959).

⁸P. Y. Yu and M. Cardona, *Fundamentals of Semiconductors* (Springer, Berlin, 1996).

⁹E. C. Heltemes and H. L. Swinney, *J. Appl. Phys.* **38**, 2387 (1967).

¹⁰E. F. Venger, A. V. Melnichuk, L. Y. Melnichuk, and Y. A. Pasechnik, *Phys. Status Solidi B* **188**, 823 (1995).

¹¹C. Nan, R. Birringer, W. Krauss, H. Gao, and H. Gleiter, *Phys. Status Solidi A* **162**, R3 (1997).

¹²M. D. McCluskey, S. J. Jokela, K. K. Zhuralev, P. J. Simpson, and K. G. Lynn, *Appl. Phys. Lett.* **81**, 3807 (2002).

¹³Y. W. Heo, L. C. Tien, D. P. Norton, B. S. Kang, F. Ren, B. P. Gila, and S. J. Pearton, *Appl. Phys. Lett.* **85**, 2002 (2004).

¹⁴W. M. Hlaing Oo, M. D. McCluskey, A. D. Lalonde, and M. G. Norton, *Appl. Phys. Lett.* **86**, 073111 (2005).

¹⁵Z. Wang, H. Zhang, L. Zhang, J. Yuan, S. Yan, and C. Wang, *Nanotechnology* **14**, 11 (2003).

¹⁶*Handbook of Optical Constants of Solids*, edited by E. D. Palik (Academic, Orlando, 1985).

¹⁷J. D. Bryan and D. R. Gamelin, *Prog. Inorg. Chem.* **54**, 74 (2005).

¹⁸D. A. G. Bruggeman, *Ann. Phys.* **24**, 636–664 (1935).

¹⁹S. Shokhovets, R. Goldhahn, V. Cimalla, T. S. Cheng, and C. T. Foxon, *J. Appl. Phys.* **84**, 1561 (1998).

²⁰D. H. Zhang, *J. Phys. D* **28**, 1273 (1995).

²¹B. H. Bairamov, A. Heinrich, G. Irmer, V. V. Toporov, and E. Ziegler, *Phys. Status Solidi B* **119**, 227 (1983).

²²M. D. McCluskey, S. J. Jokela, and W. M. Hlaing Oo, *Physica B (Amsterdam)* **376–377**, 690 (2006).

²³C. A. Wolden, T. M. Barnes, J. B. Baxter, and E. S. Aydil, *J. Appl. Phys.* **97**, 043522 (2005).

²⁴C. G. Ganqvist and O. Hundrei, *Phys. Rev. B* **16**, 3515 (1977).